

On the origin of bimodal duration distribution of Gamma Ray Bursts and the subjet model

A. Janiuk^{1*}, B. Czerny¹, R. Moderski¹, D.B. Cline², C. Matthey², S. Otwinowski²

¹*Nicolaus Copernicus Astronomical Center, Bartycka 18, 00-716 Warsaw, Poland*

²*University of California Los Angeles, Department of Physics and Astronomy, Box 951447, Los Angeles, CA 90095-1547, USA*

4 April 2018

ABSTRACT

The modified version of a bullet model for gamma ray bursts is studied. The central engine of the source produces multiple sub-jets that are contained within a cone. The emission of photons in the source frame of a sub-jet either takes part in an infinitesimally thin shell, or during its expansion for a finite time. The analysis of the observed profiles of GRBs taken by BATSE leads us to the conclusion that the latter possibility is much more favored. We also study the statistical distribution of GRBs, in the context of their bimodality of durations, taking into account the detector's capability of observing the signal above a certain flux limit. The model with shells emitting for a finite time is able to reproduce only one class of bursts, short or long, depending on the adopted physical parameters. Therefore we suggest that the GRB bimodality is intrinsically connected with two separate classes of sources.

Key words: gamma rays: bursts – gamma rays: theory

1 INTRODUCTION

The observed durations of Gamma-ray Bursts range from milliseconds to several hundreds of seconds, forming two distinct peaks. Thus two GRB classes are proposed: short ($T \leq 2$ s) and long ($T \geq 2$ s) bursts (Kouveliotou et al. 1993). (However, there have recently been claims of the third, intermediate duration peak; see Horvath et al. 2004). The collapsar scenario (Woosley 1993; Paczyński 1998) is commonly favored for the origin of a long GRB event, based on observations of afterglows and host galaxies of these events (see the review by Zhang & Meszaros 2004; Piran 2004). In particular, in some long bursts the afterglow observations clearly show the association with supernovae (Stanek et al. 2003), thus confirming the collapsar scenario. Furthermore, the GRB positions inferred from the afterglow observations are consistent with the GRBs being associated with the star forming regions in their host galaxies.

Yet, the situation is still far from clear for the short events, and various possibilities have been discussed.

An essentially different mechanism, such as a compact binary merger (Eichler et al. 1989; Paczyński 1991; Narayan, Paczyński & Piran 1992) was proposed. The duration of the central engine activity is in this case of the order of 2 seconds, appropriate to account for the fueling time of a short GRB. For many years, no optical counterpart was observed

for a short burst but the first detection of the X-ray afterglow by SWIFT satellite indicated a location 9.8 arcseconds from the center of the elliptical (type E1) galaxy (Burrows et al. 2005) at a redshift of 0.2249 ± 0.0008 (Prohaska et al. 2005). In such a galaxy strong starburst activity is not expected, and no traces of the relative supernova were found in the optical data (e.g. Kosugi et al. 2005) which again may favor a merger scenario. The results and implications for the burst GRB 050509B were recently discussed in Gehrels et al. (2005). For the recent observations of the GRB 050709, the source can be associated with the star forming galaxy at $z=0.16$ (Fox et al. 2005; Villaseñor et al. 2005), however with no supernova association in the optical lightcurve (Hjorth et al. 2005). Taking into account the distance, the luminosity of this GRB afterglow is about 3 orders of magnitude lower than for a typical long event, making the coalescing compact binary the most promising progenitor candidate (see also the discussion by Piro 2005). Furthermore, recent observation of GRB 050724 afterglow emission supports strongly the merger origin of this event (Berger et al. 2005).

Also, the events of neutron star-neutron star (NS-NS) or neutron star-black hole (NS-BH) mergers should happen quite often in the Universe (i.e. Bulik, Belczyński & Kalogera 2003; Bulik, Gondek-Rosińska & Belczyński 2004). These events should have given us a detectable sign of their presence, not only in the form of gravitational waves, but also in the gamma-rays.

On the other hand, apparently the main argument in

* E-mail: agnes@camk.edu.pl

favor of the merger scenario is that we cannot reject this possibility. Therefore there have been attempts to unify one model for all the GRBs, and assign all the bursts to the most plausible scenario, i.e. collapsar. One of the important arguments here is the observation that a short GRB may be similar to the first ~ 1 s of a long one (Ghirlanda, Ghisellini & Cellotti 2004).

It has been recently suggested (Yamazaki et al. 2004) that the bimodal duration distribution of GRBs can be explained in the frame of inhomogeneous model of a GRB jet consisting of multiple sub-jets, emitting for an infinitesimally short time. Since the sub-jets, or sub-shells, are not distributed uniformly within the main jet, but instead may have e.g. Gaussian (or power-law) distribution depending on the angular distance from the jet axis, the observer does not always detect the same number of sub-jets on his line of sight. In other words, the number of sub-jets, n_s , seen by the observer depends on the viewing angle.

The multiple sub-jet model proposed by Yamazaki et al. (2004) assumes that the duration of the observed burst does not essentially depend on the duration of activity of the central engine. Or, at least, the central engine of both short and long bursts may be of the same nature, i.e. a collapsar, operating for, say, 30 seconds. It means that duration of activity of the central engine is only slightly reflected in the duration of the observed GRB event. Instead, the event duration depends mainly on the viewing angle. This is because the observer may either detect a large number of sub-jets ($n_s > 1$), and in consequence the burst duration is long, or the number of sub-jets detected on the line of sight is $n_s = 1$ and we observe a short burst.

In this article we build a similar model of a non-uniform jet, that consists of a number of randomly distributed sub-jets. We study both the case of sub-jets emitting the gamma rays at an instantaneous time $t = t_0$, as invoked by Yamazaki et al (2004), and the case of a more realistic assumption that the emission of gamma rays is not instantaneous in time, but lasts for a certain period during the expansion of the shell from R_{\min} to R_{\max} . We calculate the profiles of individual sub-bursts as well as the total lightcurves of the GRBs that are the sum of multiple sub-bursts. Next, we fit the profiles of the individual pulses using the phenomenological prescription of Ryde & Svensson (2002) and check if these profiles correspond to these seen on the observational data from BATSE. The data were analyzed both by Ryde & Svensson (2002) in case of long duration events and by ourselves in case of short events.

We also simulate the statistical distribution of durations of the GRBs. Firstly, we hold the assumption, that only the sub-jets present on the line of sight of the observer account for the GRB event. Secondly, we release this assumption, and include also the emission from the sub-jets detected off-axis. The statistic is calculated on the basis of the condition used for classifying the events as GRB, i.e. the flux limit (the detector's capability).

In Section 2 we give the details of the model and assumptions. In Section 3.1 we present the resulting profiles of the bursts and sub-bursts and in Section 3.2 we compare these profiles with observations. In Section 3.3 we show the statistical distributions of the burst durations that result from the multiple sub-jet model. Finally, in Section 4 we discuss our results and give conclusions.

2 MODEL

2.1 Geometry

We consider a collimated jet in the form of a cone with the opening angle $\Delta\theta_{\text{tot}}$, which is present for the whole period of the duration of central engine activity, T_{dur} . The main jet consists then of a number N_{sub} of sub-jets, which have smaller opening angles $\Delta\theta_{\text{sub}}$ and are launched at their characteristic departure times, extending until the time T_{dur} : $0 < t_{\text{dep}} < T_{\text{dur}}$. The position of each sub-jet is determined by two angles, (θ_i, φ_i) , such that the angular distribution of the direction θ_i , i.e. the distance from the z axis of the main jet, is given by the Gaussian function:

$$P(\theta_i)d\theta_i = e^{-\frac{1}{2}\frac{\theta_i^2}{\theta_c^2}} d\theta_i, \quad \text{for } \theta_i < \Delta\theta_{\text{tot}} - \Delta\theta_{\text{sub}} \quad (1)$$

where $\theta_c < \Delta\theta_{\text{tot}}$ is a parameter of this distribution. Independently, the angle φ_i , measured in the $x - y$ plane in the basis of the jet, is uniformly distributed between 0 and 2π .

We assume that all the subjets have the same Lorentz factors γ and up to the radius r_0 , for a period of time t_0 , expand in a photon-quiet phase. At the radius r_0 the photons are emitted instantaneously, i.e. the duration of the photon-active phase in the comoving frame is infinitesimally small. The sub-jet i is expanding for the time:

$$t_0^i = t_{\text{dep}}^i + \frac{r_0}{c\beta} \quad (2)$$

where $\beta = \sqrt{1 - 1/\gamma^2}$. Then, all the photons are emitted in an infinitesimally short time, at:

$$t_{\text{em}}^i = \frac{r_0}{c\beta} \quad (3)$$

after the launch of a sub-jet.

The observer's position is determined by his viewing angle $(\theta_{\text{obs}}, \varphi_{\text{obs}})$, as measured in the reference frame of the main jet. Again, we randomly choose these angles, without favoring any particular direction, and the angles are $0 < \theta_{\text{obs}} < \Delta\theta_{\text{tot}}$ and $0 < \varphi_{\text{obs}} < 2\pi$. The observed temporal structure of a flash of radiation produced by a sub-jet is determined by the time measured in the observer's frame, i.e. the arrival time of a photon:

$$T_{\text{obs}}^i = (1 + z)(t_0^i + t_{\text{em}}^i(1 - \beta \cos \lambda)) \quad (4)$$

where we take into account that relativistic aberration of photons emitted at an angle λ to the observer occurs only after the expansion time t_0^i . This is because the assumed radius of the emitting photosphere is large and cannot be neglected. Here the angle λ is measured between the direction of motion of the emitting plasma with respect to the observer.

Because of the axial symmetry of the problem we choose an observer to be located at $\varphi_{\text{obs}} = 0$ in the reference frame of the jet. In order to determine this angle λ and its dependence on the observer's position, location of the sub-jet, and direction of the photon, let us consider a spherical triangle located on the surface of the sphere of the radius r_0 . The vertexes of this triangle are determined by the directions of the jet axis, observer's axis, and sub-jet axis. Therefore the sides of the triangle are θ_{obs} , θ_i , and λ_i , while the angle opposite to λ_i is φ_i (see Figure 1).

This implies the dependence:

$$\cos \lambda_i = \cos \theta_i \cos \theta_{\text{obs}} + \sin \theta_i \sin \theta_{\text{obs}} \cos(\varphi_{\text{obs}} - \varphi_i) \quad (5)$$

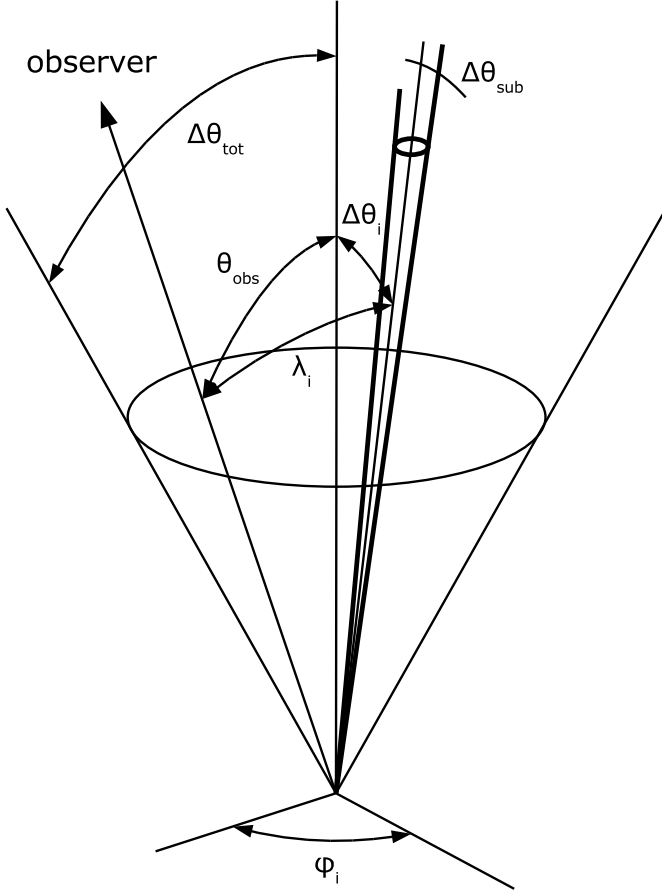


Figure 1. Geometry of the problem. The jet has a half-opening angle $\Delta\theta_{\text{tot}}$. The observer is located at $(\varphi_{\text{obs}} = 0, \theta_{\text{obs}})$ in the jet reference frame. Each sub-jet has a half-opening angle $\Delta\theta_i$ and is located at (φ_i, θ_i) . The angle between the observer and the sub-jet axis, λ_i , form a spherical triangle together with the angles θ_{obs} and θ_i .

Now, the maximal and minimal angle λ between the direction of motion of the emitting plasma with respect to the observer, is given by:

$$\lambda_{\text{max}} = \lambda_i + \Delta\theta_{\text{sub}} \quad (6)$$

$$\lambda_{\text{min}} = \min(0; \lambda_i - \Delta\theta_{\text{sub}})$$

Having calculated the angle λ_i , we can determine the time T_{obs} at which the photon hits the detector. The duration of a single sub-burst is therefore given by the difference between the ending and starting times in the observer's frame:

$$T_{\text{start}}^i = T_0^i + (1+z) \frac{r_0}{c\beta} (1 - \beta \cos \lambda_{\text{min}}) \quad (7)$$

$$T_{\text{end}}^i = T_0^i + (1+z) \frac{r_0}{c\beta} (1 - \beta \cos \lambda_{\text{max}})$$

where $T_0^i = (1+z)t_0^i$.

In the above considerations, for simplicity we neglect the dependence of the angle λ between photon's direction and observer's position on the angle φ_{obs} . This is because we have random observers uniformly distributed between 0 and 2π , so for a sample with large enough statistics this will not influence the results. Also, please note that we did not give

an exact formula for the angle λ but rather its upper and lower limits resulting from the opening angle of a sub-jet. The derivation of an exact expression would require a transformation between the two reference frames: jet's (in which the observer's position is given) and sub-jet's (in which the photons from a single sub-jet are produced).

Therefore the simplified condition for the observer's position to fall inside the sub-jet is:

$$\lambda_i \leq \Delta\theta_{\text{sub}}. \quad (8)$$

and also neglects the dependence on the angle φ .

2.2 Duration of a burst

If the line of sight of the observer coincides with only one sub-jet, then the duration of this sub-jet is equivalent to the duration of the GRB. Alternatively, the observer may 'catch' a number of sub-jets. In this case the duration of the GRB is the sum of durations of all the sub-bursts that coincide with the line of sight:

$$\Delta T = \text{Max}(T_{\text{end}}^i) - \text{Min}(T_{\text{start}}^i) \quad (9)$$

The absolute maximal and minimal duration of a GRB event are estimated as follows. The duration of a single sub-burst for $\lambda_i > \Delta\theta_{\text{sub}}$ is:

$$\begin{aligned} c\Delta t &= r_0(\cos(\lambda_i - \Delta\theta_{\text{sub}}) - \cos(\lambda_i + \Delta\theta_{\text{sub}})) \\ &= 2r_0 \sin \lambda_i \sin \Delta\theta_{\text{sub}} \end{aligned} \quad (10)$$

while for $\lambda_i < \Delta\theta_{\text{sub}}$ it is:

$$c\Delta t = r_0(1 - \cos(\lambda_i + \Delta\theta_{\text{sub}})) \quad (11)$$

(cf. Eq. 5). Therefore the shortest possible sub-bursts are these seen on-axis ($\lambda_i = 0$), and:

$$\Delta t_{\text{min}} \approx \frac{r_0}{c} \frac{1}{2} (\Delta\theta_{\text{sub}})^2 \quad (12)$$

For our standard parameters, $r_0 = 10^{14}$ cm and $\Delta\theta_{\text{sub}} = 0.02$, equation (12) gives $\Delta t_{\text{min}} = 0.66$ s.

The longest theoretically possible burst would be seen at the angle $\lambda_i = \pi/2$, and when the sub-bursts caught on the line of sight were so numerous that they would cover the whole jet opening angle: instead of $\Delta\theta_{\text{sub}}$ we take $\Delta\theta_{\text{tot}}$. In case of our parameters ($\Delta\theta_{\text{tot}} = 0.2$, $T_{\text{dep}} = 30$ s) this is about 1350 s. In practice, as discussed in the next section, the light aberration will effectively limit the observed surface to within a small angle around the line of sight. In such a case the duration of the longest burst will strongly depend on the central engine lifetime T_{dep} and on the sensitivity of the instrument used to observe the burst."

2.3 Sub-burst profiles

The duration of the GRB event depends not only on the number of sub-jets that are observed, but also on the energy flux that is measured by the detector. This is of particular importance if we allow also for the sub-bursts that are observed off-axis, to contribute to the observed spectrum. Because the energy flux observed from the relativistic jet sharply decreases for the viewing angles that are outside the jet cone, only a part, if at all, of such a sub-burst could be classified as a gamma ray burst.

The energy flux emitted from an expanding shell, as seen by the distant observer located on the jet axis, was studied in Fenimore et al. (1996). They considered both the case of an infinitesimally thin and extended shell.

The photons emitted from a relativistically expanding shell, that arrive to the observer at the same time, originate from a prolate ellipsoid (Rees 1966). In order to calculate the flux in the detector rest frame, we have to integrate the emitted spectrum over the surface resulting from the cross-section of the ellipsoid with the sphere of the center in the detector and radius equal to the distance to the source:

$$dF_\nu(T) \propto \oint f(\nu') \delta^3 dA \quad (13)$$

where $\delta = [\gamma(1 - \beta \cos \theta)]^{-1}$ is the Doppler factor, $f(\nu')$ is the emissivity in the comoving frame, and $\nu' = (1+z)\nu\gamma(1 - \beta \cos \theta)$. The surface differential is determined by:

$$dA = \frac{1}{D^2} \Delta \Phi \sin \theta d\theta \quad (14)$$

where

$$\Delta \Phi = \pi \quad \text{if } \theta < (\Delta \theta_{\text{sub}} - \theta'_{\text{obs}}) \text{ or } \theta_{\text{obs}} = 0. \\ \Delta \Phi = 2 \arccos\left(\frac{\cos \Delta \theta_{\text{sub}} - \cos \theta \cos \theta'_{\text{obs}}}{\sin \theta \sin \theta_{\text{obs}}}\right) \quad \text{otherwise} \quad (15)$$

The angle $\theta'_{\text{obs}} \equiv \lambda_i$ is between the direction to the observer and the sub-jet axis. The angle θ depends on time in the observer's frame, and here is how the observed pulse varies with time:

$$\theta(T) = \arccos\left(\frac{1}{\beta} - \frac{1}{1+z} \frac{c}{r}(T - T_0)\right) \quad (16)$$

We calculate the pulse profile for $T_{\text{start}} < T < T_{\text{end}}$, and in principle we should integrate from θ_{min} to θ_{max} (where $\theta_{\text{min}} = 0$ if $\theta'_{\text{obs}} < \Delta \theta_{\text{sub}}$ or $\theta_{\text{min}} = \theta'_{\text{obs}} - \Delta \theta_{\text{sub}}$ otherwise, and $\theta_{\text{max}} = \theta'_{\text{obs}} + \Delta \theta_{\text{sub}}$). However, in case of an infinitesimally thin shell, we must keep $r = r_0$ and only one value of θ will satisfy the relation 16. In other words, the integral in equation 13 becomes one-dimensional integral over the arc of the length $\Delta \phi$.

2.4 Shell emission for a finite time in the comoving frame

The model described above considered the emission that is infinitesimally short in the comoving frame, and the duration of the observed pulse is a result of the purely geometrical transformation to the observer's frame. In reality, the emission from the expanding shell may not be instantaneous, but rather lasts for a certain time. In our model the duration of the emission is determined by the minimum and maximum radii of the expanding shell, r_{min} and r_{max} . The starting and ending time of an individual sub-burst in the observer's frame is given by:

$$T_{\text{start}}^i = (1+z)(t_{\text{dep}}^i + \frac{r_{\text{min}}}{c\beta}(1 - \beta \cos \lambda_{\text{min}})) \quad (17) \\ T_{\text{end}}^i = (1+z)(t_{\text{dep}}^i + \frac{r_{\text{max}}}{c\beta}(1 - \beta \cos \lambda_{\text{max}}))$$

where λ_{min} and λ_{max} are given by the equations 6. In order to obtain the time profile of each sub-burst, we have to calculate the integral in Eq. 13, over θ and $\Delta \phi$, where the limits for $\theta(T)$ will satisfy the condition $r_{\text{min}} < r < r_{\text{max}}$. In

this way we sum up in the observer's frame all the photons that are emitted in different moments in the expanding shell between r_{min} and r_{max} but arrive to the detector at the same time T .

2.5 Comparison with previous work

The idea of the GRB jets consisting of multiple sub-jets was proposed by Heinz & Begelman (1999), and recently modeled in detail by Yamazaki et al. (2004) and Toma et al. (2005). In the latter work the authors successfully reproduced the bimodal distribution of the GRB durations. Here we basically follow the same scheme of the multiple sub-jet model, however there are a few differences.

(i) First, we calculate the angles between the emitting electrons and observer's direction, explicitly taking into account the sub-jet azimuthal angle, φ_i (see equation 5 and Fig. 1).

(ii) Secondly, we distinguish between the cases with and without the off-axis emission included in the total GRB pulse. This is particularly important, when determining the duration of a short burst and statistical fraction of short bursts in the simulation.

(iii) Therefore, thirdly, we adopt a different way of selecting the pulses that are responsible for gamma ray signal. Instead of the spectral hardness, we adopt a criterion based on the sufficient signal with respect to the background flux. The minimum flux is inversely proportional to the square root of T_{90} , as implied by the BATSE characteristics (see Section 3.3.2).

(iv) Finally, we include in the model the possibility of a non-instantaneous emission, in the expanding shell that emits radiation from R_{min} to R_{max} .

3 RESULTS

3.1 Pulse profiles

We present here the shapes of the profiles for individual sub-bursts as well as the total GRB events that consist of multiple sub-jets. First, we show the results for the case of an infinitesimally thin emitting shell. In this case the emission in the source frame is instantaneous, and the duration of the event is determined only by the geometry.

3.1.1 Profiles for the infinitesimally thin shell emission

In Figure 2 we show the exemplary profiles of the pulses from the individual sub-jets, as seen by the observer. The sub-jet opening angle is $\Delta \theta_{\text{sub}} = 0.02$ and therefore the pulses that are seen inside this opening angle are much more energetic. The pulses seen off-axis are weaker, due to the strong dependence of the flux on the Doppler factor and in turn on the viewing angle. This means that the maximum of the observed flux is almost an order of magnitudes lower, as soon as the observer is located outside $\Delta \theta_{\text{sub}}$ (see e.g. cases of $\theta'_{\text{obs}} = 0.018$ and $\theta'_{\text{obs}} = 0.023$). On the other hand, for larger viewing angles the pulse duration, as well as its starting time, substantially increase. For $\theta_{\text{obs}} = 0.007$ a break in the light curve is caused by the conical geometry of the jet as discussed by Rhoads (1997).

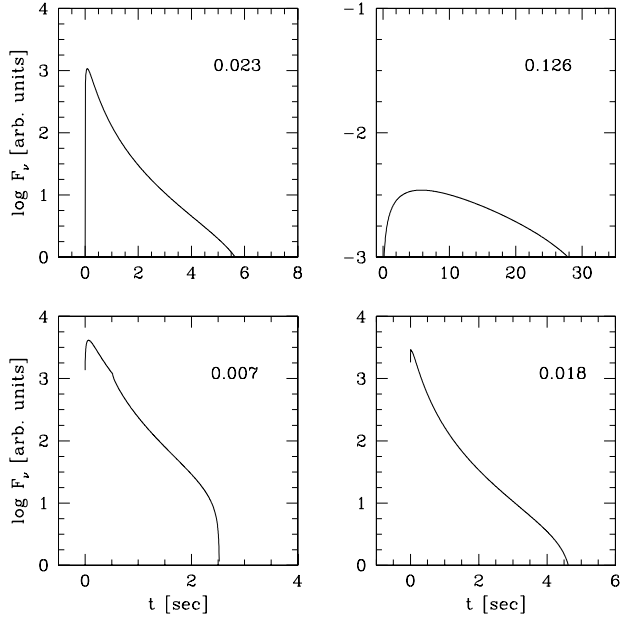


Figure 2. The exemplary pulse profiles emitted from the individual sub-jets as seen by the observers located at various lines of sight. The angle $\theta'_{\text{obs}} = 0.007, 0.018, 0.023$ and 0.126 is indicated in each panel. The sub-jet opening angle is always $\Delta\theta_{\text{sub}} = 0.02$ and the Lorentz factor is $\gamma = 100$. The flux is given with arbitrary normalization and essentially does not depend on frequency (flat spectrum).

In Figure 3 we show the total profiles of GRB, which are the result of multiple pulses seen by the observer. The plots are labeled here with the observer angle with respect to the axis of the jet. While looking at small θ_{obs} , the observer will detect a large number of sub-pulses that overlap, and give rise to a long, variable GRB. In contrast, the observer looking at larger angle θ_{obs} , can detect only a few sub-pulses. These form either a set of separate narrow spikes, or are connected with each other by the emission from these sub-bursts that were seen only off-axis (see Section 3.3.2 and condition Eq. 21 for the detection of the off-axis emission).

The spectrum in the comoving frame is defined using the broken power law function (see also the formula in Band et al. 1993):

$$f_{\nu'} = (\nu'/\nu'_0)^{1+\alpha} \quad \text{for} \quad \nu' < \nu'_0 \\ (\nu'/\nu'_0)^{1+\beta} \quad \text{for} \quad \nu' > \nu'_0 \quad (18)$$

In the comoving frame the break frequency is assumed $\nu'_0 = 2\text{keV}$, and the spectral indices are $\alpha = -1$ and $\beta = -3$ (the averaged values of the observed spectral indices were given e.g. by Pendleton et al., 1994; Preece et al. 1998, 2000). The lightcurves in Fig. 3 are plotted in 4 energies: 1.41, 112, 482 and 2070 keV.

3.1.2 Emission from the thick expanding shell

Now, we show the results for the case of a thick expanding shell. In this case the duration of the individual pulse is determined not only by the geometry but also by the duration of the emission in the source frame.

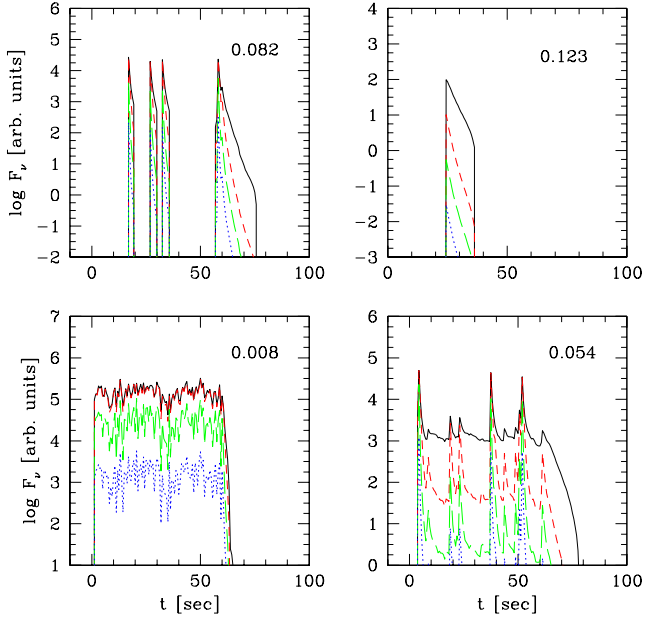


Figure 3. Profiles of the GRBs for various observing angles with respect to the main jet axis: $\theta_{\text{obs}} = 0.008, 0.054, 0.082$ and 0.123 . The lightcurves are plotted in 4 energies: 1.41 (solid line), 112 (short dashed line), 482 (long-dashed line) and 2070 keV (dotted line). The bursts contain the total emission (on and off-axis) from the sub-jets, emitting at $r_0 = 10^{14}$ cm, that satisfy the condition Eq. 21 (see text).

In Figure 4 we plot several examples of the individual sub-bursts, for various observing angles with respect to the sub-jet axis: $\theta'_{\text{obs}} = 0.004, 0.017, 0.024$ and 0.127 .

In Figure 5 we plot the total GRBs, consisting of multiple sub-pulses, for several exemplary values of the observers angle (with respect to the main jet axis): $\theta_{\text{obs}} = 0.009, 0.044, 0.096$ and 0.128 . The Figure shows the lightcurves in 4 energies: 1.41, 112, 482 and 2070 keV. The jet opening angle is $\Delta\theta_{\text{tot}} = 0.2$. For the bursts that are observed close to the edge of the cone (large θ_{obs}), the probability of detecting a sub-jet on-axis is very small. These bursts consist mostly of the off-axis emission from the sub-jets, typically either with one-two strong, on-axis pulses (case of $\theta_{\text{obs}} = 0.096$) or with none on-axis pulse (case of $\theta_{\text{obs}} = 0.128$). These bursts have the longest total durations and last for several hundreds of seconds. The bursts that are observed closer to the main jet axis, are stronger and more variable, and their durations typically range up to ~ 100 seconds.

3.2 Fitting the pulse profiles

The observed profiles of GRBs can be fitted to the exponential function in the rise phase:

$$N(t) \propto \exp(mt) \quad (19)$$

and to the power law shape in the decay phase (Ryde & Svensson 2002):

$$N(t) \propto (1 + t/\tau)^n \quad (20)$$

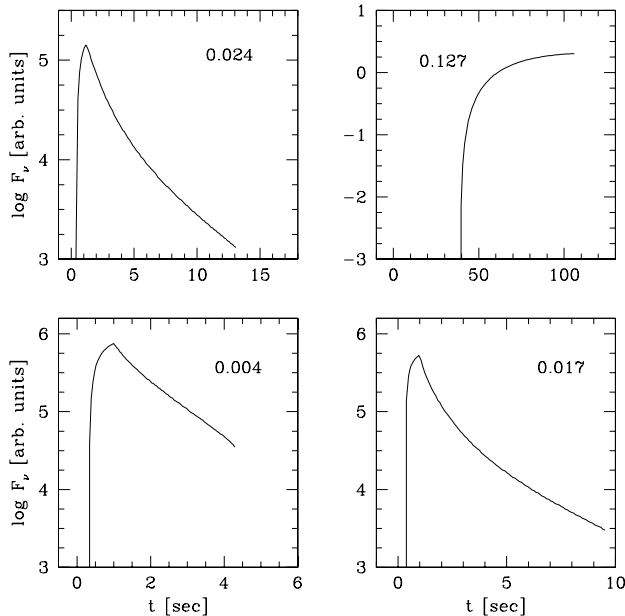


Figure 4. Profiles of the individual sub-bursts for various observing angles with respect to the sub-jet axis: $\theta'_{\text{obs}}=0.004, 0.017, 0.024$ and 0.127 . Thick expanding shell approach.

where m, n and τ are the free parameters. As shown by Ryde & Svensson (2002) for a sample of BATSE data, the distribution of the index n , characteristic for the pulse decay phase, peaks twice: around $n = 1$ and $n = 3$. However, one should keep in mind that this observational result has been obtained using a limited statistics of ~ 20 long GRBs detected by BATSE. Here we fit the pulse profiles that are obtained from the sub-jet model.

First, we fit the pulses resulting from the assumed delta-function emission ($t = t_0, r = r_0$) in the comoving frame. In the Figure 6 we show the distribution of indices for the sub-pulses that fitted to this pulse profile, and for which the maximum gamma-ray flux was substantially large (this corresponds roughly to the observing angle $\theta'_{\text{obs}} > 0.03$). The indices in our distribution are in the range $n = 4 - 6$, while neither $n = 1$ nor $n = 3$ showed up, contrary to the results obtained by Ryde & Svensson (2002).

Next, we fit the pulses resulting from the assumed emission in the expanding shell from R_{min} to R_{max} . In the Figure 7 we show the distribution of indices for all the sub-pulses that fitted to this pulse profile (again apart from the sub-jets seen at angles $\theta'_{\text{obs}} > 0.03$). The distribution is now much broader, with certain enhancement at low values of n , but with no traces of $n = 3$ secondary peak, as found by Ryde & Svensson (2002).

3.2.1 New sample from BATSE

Here we present the analysis of the new sample of BATSE data, in order to make further observational tests for the model. Now, contrary to Ryde & Svensson (2002), we study only the short duration bursts. The sample of bursts is listed in Table 1 and contains 83 GRBs, of durations from 0.067 s to 1.954 s. The data from the energy band 50 – 300 keV

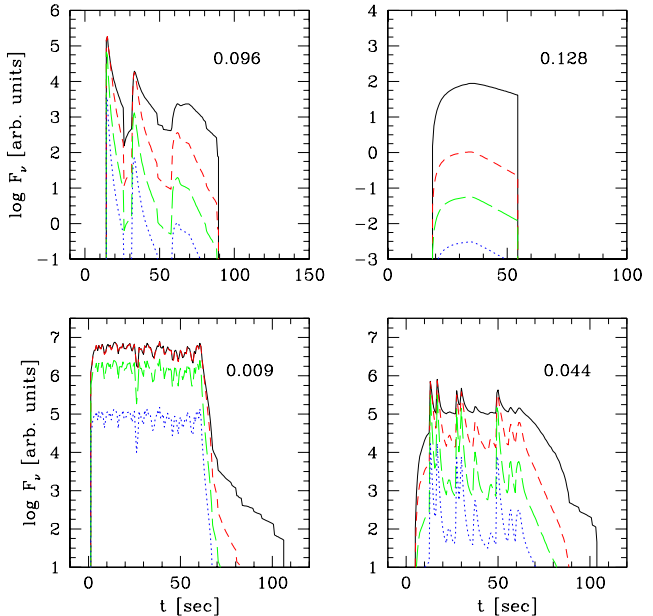


Figure 5. The same as in Fig. 3; the observing angles are: $\theta_{\text{obs}}=0.009, 0.044, 0.096$ and 0.128 . The bursts contain the total emission (on and off-axis) from the sub-jets, from $R_{\text{min}} = 10^{14}$ cm to $R_{\text{max}} = 2 \times 10^{14}$ cm.

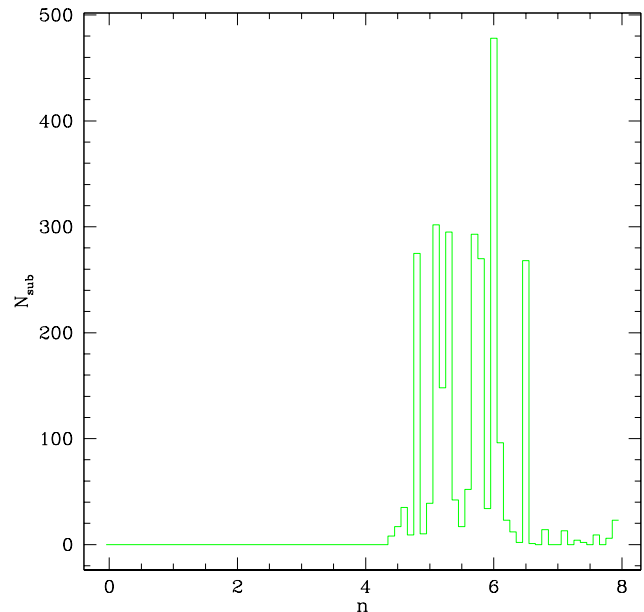


Figure 6. The distribution of the index n , fitted to the sub-pulses profiles due to the instantaneous emission at $r = r_0$.

were used and the bursts were selected so that the signal to noise ratio in this band was larger than 10.

We fit the pulse profiles to the shape defined by the equation 20. The data are in units of [cts/s] and we do not convert them to the photon flux, due to the large er-

Trigger	T_{90}	S/N	χ^2	τ	n	Trigger	T_{90}	S/N	χ^2	τ	n
207	0.085	16.77	1.83	0.016	2.43	3502	0.416	19.62	1.01	0.011	0.93
480	0.067	31.04	1.44	0.046	4.50	3644	0.776	38.84	1.22	0.276	3.18
512	0.183	15.82	1.40	0.006	1.92	3668	0.176	20.41	1.45	0.061	1.89
788	0.303	15.50	0.84	0.261	5.58	3751	0.535	18.05	0.85	0.036	1.14
830	0.131	31.96	1.26	0.421	9.15	3810	0.076	10.71	0.87	0.006	1.35
906	0.398	15.73	1.04	0.056	2.70	3867	0.939	22.81	0.88	0.021	1.02
1102	0.187	18.34	1.11	0.041	1.68	3940	0.576	17.16	1.06	0.006	1.02
1112	0.442	32.14	1.39	0.246	2.16	5206	0.304	29.00	1.78	1.051	7.95
1154	0.193	18.59	1.69	0.006	0.69	5469	1.504	27.83	0.87	0.011	0.63
1223	0.974	10.08	0.67	0.021	0.87	5499	0.624	18.02	0.72	0.011	1.32
1308	0.215	10.71	0.86	0.021	1.83	5528	0.855	19.96	1.34	0.011	0.72
1463	0.192	21.99	0.81	0.051	2.40	5529	1.015	25.29	1.21	0.016	0.90
1694	0.388	17.83	1.68	0.006	0.72	5547	0.896	23.55	1.17	0.006	0.48
2126	0.401	25.30	0.99	0.006	0.75	5592	0.475	10.13	0.96	0.006	0.66
2132	0.090	10.70	0.60	0.096	6.03	5633	0.253	15.98	1.55	0.006	0.84
2201	0.380	11.10	0.76	0.121	3.21	6123	0.186	48.11	1.39	0.301	7.50
2206	0.602	11.80	0.85	0.016	0.81	6145	0.460	18.65	1.18	1.076	10.95
2220	0.951	14.06	0.79	0.006	0.90	6215	0.640	13.28	1.09	0.011	0.75
2268	1.954	21.63	0.82	1.496	8.19	6230	1.280	12.04	0.71	0.201	5.46
2377	0.496	41.49	1.25	0.091	2.64	6265	0.199	27.99	0.83	0.271	7.26
2502	0.512	13.24	0.91	0.071	1.47	6299	0.202	18.20	1.17	0.041	1.95
2512	0.359	19.42	0.96	0.176	4.23	6347	0.448	11.25	0.88	0.006	0.69
2564	0.256	10.33	0.83	0.011	1.02	6372	0.768	14.55	0.81	0.051	1.35
2597	0.256	10.90	1.02	0.006	0.78	6385	0.896	14.02	0.74	0.026	3.00
2632	1.443	22.19	0.78	0.006	0.63	6386	0.832	17.96	0.96	0.006	0.69
2649	0.256	14.79	1.23	0.011	0.90	6569	0.936	10.45	0.78	0.006	0.81
2755	0.144	11.10	0.74	0.171	5.04	6573	0.289	12.75	0.99	0.011	0.99
2788	0.872	25.63	0.87	0.011	0.84	6591	0.773	22.82	1.01	0.011	0.81
2861	1.599	12.87	0.73	0.071	1.92	6689	0.192	16.38	0.88	0.021	1.41
2892	0.288	11.95	0.90	0.051	1.77	6693	0.283	20.10	1.37	0.036	1.38
2896	0.456	51.35	0.72	0.276	5.34	6700	0.192	15.33	1.42	0.461	8.58
2918	0.448	16.47	0.87	0.056	2.13	7060	0.146	14.04	0.74	0.071	3.06
2952	0.680	35.08	1.29	0.021	1.47	7173	0.966	22.50	1.20	0.006	0.57
2977	0.576	15.12	1.18	0.016	0.93	7227	0.092	12.30	1.07	0.156	3.84
3066	0.176	16.18	1.15	0.011	0.93	7292	0.262	26.31	1.06	0.396	6.24
3078	0.224	17.94	1.47	0.006	0.84	7813	0.564	32.57	0.97	0.371	3.57
3121	0.792	11.76	0.90	0.006	0.60	7939	1.039	57.77	0.79	0.006	0.27
3282	0.078	14.13	1.15	0.021	2.07	7970	0.387	11.37	0.89	0.006	0.87
3323	0.448	14.77	0.92	0.006	0.72	7988	0.413	16.21	0.83	0.131	4.62
3338	0.108	12.32	1.03	0.111	6.33	7995	0.608	11.52	0.68	0.026	1.38
3340	1.016	16.30	1.04	0.016	0.99	8047	0.892	32.19	1.33	0.021	0.60
3359	0.344	25.65	1.19	0.056	1.59	8076	0.218	12.31	0.82	0.226	6.57
3379	0.608	22.48	0.98	0.006	0.60						

Table 1. Sample of the short GRBs observed by BATSE. The bursts were selected on the basis of their signal to noise ratio, $S/N > 10$, in the energy band 50-300 keV. The total sample contained 182 bursts; the table lists only these bursts that fitted to the defined profile shape (Eq. 20).

ror bars in case of short bursts. The conversion to physical units would dramatically increase the uncertainty.

In the Figure 8 we show the distribution of the index n in the observed sample. The plot contains only these bursts, that fitted to the defined profile shape. Only less than half of the originally selected bursts remained (83 out of 182).

As the Figure shows, no significant excess in the distribution is seen around the index $n = 3$. However, an excess at low values of n is seen quite clearly. The figure shows overall similarity to the theoretical prediction based on thick shell approximation while it is definitively different from Figure 6.

3.3 Statistical distribution of bursts

Below we show the results of the Monte Carlo calculations of the statistical distribution of GRB durations. In all the simulations we take $N_{\text{obs}} = 1000$ observers (or, equivalently, 1000 GRBs at different positions on the sky with respect to the observer). Each of the bursts consists of $N_{\text{sub}} = 350$ sub-jets, which have the opening angles of $\Delta\theta_{\text{sub}} = 0.02$ and Lorentz factor $\gamma = 100$. The departure time of each sub-jet, t_{dep} , is chosen randomly within the total activity time of the central engine, i.e. between 0 and $T_{\text{dur}} = 30$ sec. The sub-jets have a quasi-Gaussian distribution within the jet of the total opening angle $\Delta\theta_{\text{tot}} = 0.2$.

We compare the results for two cases: the instantaneous emission from a thin shell at $r = R_0$ and the emission from

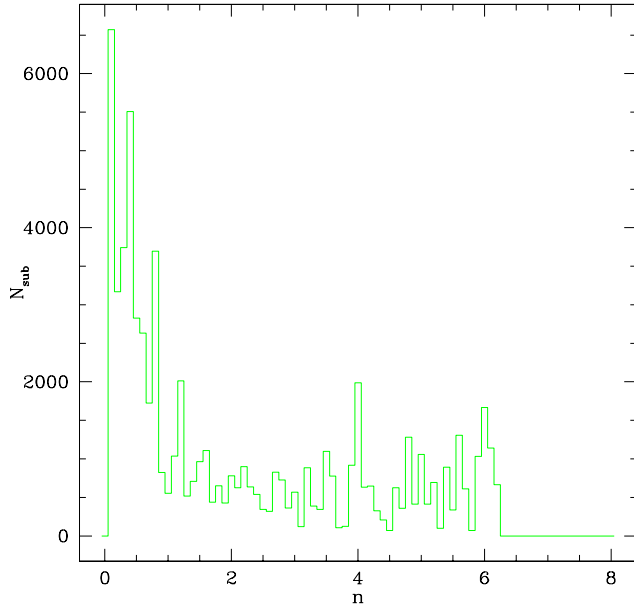


Figure 7. The distribution of the index n , fitted to the sub-pulses profiles due to the emission from the expanding shell from $R_{\min} = 10^{14}$ cm to $R_{\max} = 2 \times 10^{14}$ cm.

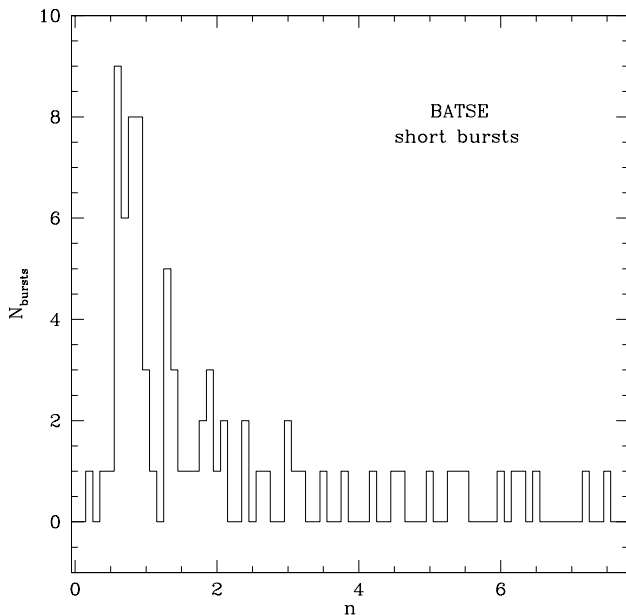


Figure 8. The distribution of the index n , fitted to the profiles of the short GRBs observed by BATSE.

the thick expanding shell, from $r = R_{\min}$ to $r = R_{\max}$. The infinitesimally thin emitting shell is located at $r_0 = 10^{14}$ cm, and the thick shell emits the radiation from $R_{\min} = 10^{14}$ cm, to $R_{\max} = 2 \times 10^{14}$ cm. Below, in the Section, 3.3.1, we discuss the distribution limited to these bursts that contain only the sub-jets, and in Section 3.3.2 we show the results for the bursts that include the emission from every sub-pulse,

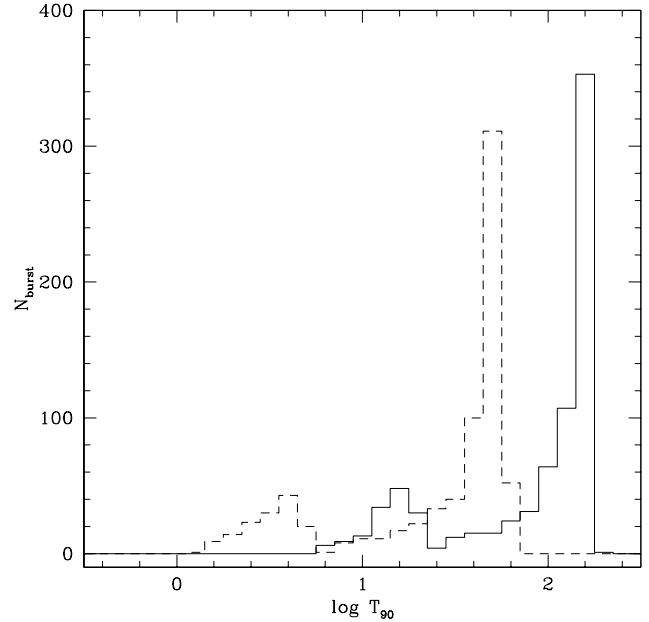


Figure 9. The simulation with $N_{\text{obs}} = 1000$ random observers, and the jet consisting of $N_{\text{sub}} = 350$ sub-jets. The histogram shows the number of bursts (observer's positions) in the function of the total burst duration time. Each burst includes only the sub-jets caught on the line of sight. The emission is produced either by an extended shell from $R_{\min} = 10^{14}$ cm, to $R_{\max} = 2 \times 10^{14}$ cm (solid line) or by the thin shell at $r_0 = 10^{14}$ cm (dashed line).

seen either on axis or off-axis. The criterion for counting these sub-bursts as a part of the GRB is their flux above a background for the duration time T_{90} , as observed by the BATSE detector.

3.3.1 Statistics for nearly-on-axis observers

As a first step, we will study the distribution of burst durations under the (restrictive) assumption that only the sub-jets that are on the line of sight contribute to the GRB event. In other words, we neglect any emission that is observed off-axis, which could possibly contribute to gamma rays, assuming that those events would only give rise to the X-ray Flashes. We require that all the sub-jets that are contributing to the GRBs will satisfy the condition 8 with respect to the observer axis.

The observer may catch a sub-jet on his line of sight either while looking very close to the main jet axis, with $\theta_{\text{obs}} \sim 0$ (multiple sub-jets are seen), or while looking close to the edge. In the first case, the number of detected sub-jets is about 300, and in the latter case, the observer is most likely to catch one sub-jet (about 10% of observers). Obviously, the largest number of observers do not catch any single sub-jet.

In the Figure 9 we show the histogram of burst durations, for this simulation. The distribution has two peaks, located around 4 and 50 seconds, or 8 and 65 seconds, for an instantaneous or extended emission from the sub-jets, respectively. The exact location of the peaks depend on the

model parameters, and in particular the short GRB peak is sensitive to the value of the radius of emitting shell, as well as the opening angle of a sub-jet (cf. Eq. 12). For example, $\Delta\theta_{\text{sub}} = 0.015$ shifts the short burst duration peak to $T_{90} = 2.5$ s, while the radius of $r_0 = 10^{13}$ cm shifts this peak to $T_{90} = 0.4$ s. The long burst peak does not depend on these parameters, but rather on the duration time of the central engine activity. If we take $T_{\text{dur}} = 0.3$ s, instead of 30 s, the peak for long bursts is shifted to $T_{90} = 8$ s. However, the peak for short GRBs does not change and is located at ~ 4 s, so the shorter activity time results in the essentially single-peak distribution for only short bursts.

3.3.2 Statistics for the off-axis emission included

In this section we discuss the effect of the off-axis emission that contributes to gamma rays. Since the observed flux drops very rapidly with the increasing inclination of the line of sight, as soon as the observer axis is located outside the sub-jet cone, it is crucial to determine the condition for the GRB to be observed. This is connected mainly with the flux limit of the detector.

For example, BATSE will generate a burst trigger if the count rate in two or more detectors exceeds a threshold specified in units of standard deviations above background (nominally 5.5). The actual detection depends only slightly on the spectral hardness

In the Figure 10 we show the results of the simulation. The off-axis emission of the sub-jets contributes to GRB whenever

$$F_{10\text{keV}}^{\text{peak}} > 5.5 \times \sqrt{F_{\text{B}}/T_{90}}. \quad (21)$$

where the background flux is arbitrarily chosen to be $F_{\text{B}} = 1.0$

The shortest GRBs are mainly due to the bursts that include only the off-axis emission. This is because the weak off-axis sub-bursts in general tend to have longer durations, which sometimes prevents them from falling below the threshold. On the other hand, the weakest of these sub-bursts have too small flux at 100 keV, and are missed anyway. Therefore the total number of the sub-bursts that contribute to the left wing of this histogram is small and the only sub-bursts that are counted here are the off-axis sub-bursts.

The sub-bursts caught on-axis (or nearly on-axis) give the main contribution to the longest GRBs. Since their emitted flux is always large, the threshold limit does not affect them. These sub-bursts are seen mostly at very small observing angle θ_{obs} , and a large number of them is detected. This means a large spread between the starting time of the first sub-jet and ending time of the last one, which translates into a long total event.

The shape of the histogram is clearly not bimodal. A small excess of short bursts around $T \sim 10$ s appears only for the model with instantaneous emission at $r = r_0$, however this feature disappears already in the model with expanding shell emission from r_{min} to r_{max} . The bimodal distribution is found by Toma et al. (2005) in the model with only instantaneous emission at $r = r_0$. However, these authors consider the case when the events are classified by the detector as a GRB on the basis of their spectral hardness. They select only these events for which the hardness ratio, i.e. the ratio

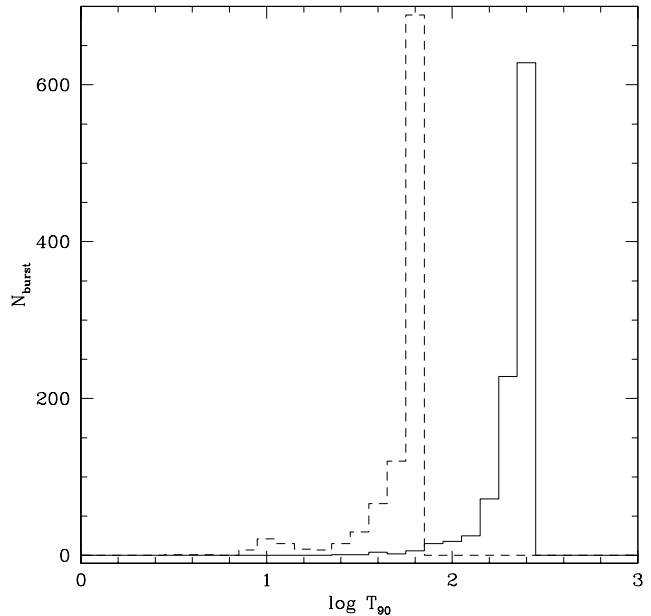


Figure 10. The results of the simulation with the emission from off-axis sub-jets included. The bursts include only these off-axis sub-bursts, for which $F_{10\text{keV}}^{\text{peak}} > 5.5 \times \sqrt{F_{\text{B}}/T_{90}}$. Other parameters are the same as in Fig. 9.

of fluency defined as $S_{\nu_1, \nu_2} = \int_{T_{\text{start}}}^{T_{\text{end}}} \int_{\nu_1}^{\nu_2} F_{\nu} d\nu dT$, is smaller than $S_{2\text{keV}, 30\text{keV}}/S_{30\text{keV}, 400\text{keV}} \approx 0.3$. In this case the contribution from the short bursts is much more pronounced.

3.3.3 Distribution of redshift

The distribution of the long bursts with redshift is now thought to trace the star formation in an unbiased way (Jakobsson et al. 2005). Therefore the probability of finding a bursts with a redshift z is given by:

$$dP(z) = AD^2 R(z) dz \frac{dr}{dz} \quad (22)$$

where $R(z)$ is the star formation rate in the comoving frame (Porciani & Madau 2001), D is the cosmological distance (Chdrowski 2005), A is the normalization constant and $dr/dz = c/H_0/\sqrt{\Omega_{\text{M}}(1+z)^3 + \Omega_{\Lambda}}$. We adopt the cosmological parameters of $\Omega_{\text{M}} = 0.3$, $\Omega_{\Lambda} = 0.7$ and $H_0 = 65$. The normalization is calculated from the condition that:

$$\int_{z_{\text{min}}}^{z_{\text{max}}} P(z) dz = 1. \quad (23)$$

Here we check the influence of the redshift distribution on our model. For each of the 1000 bursts we randomly choose its redshift, within a distribution with a cut-off at $z_{\text{max}} = 4$. The Figure 11 shows the resulting statistics of bursts.

The duration distribution is now more smeared than in case of a constant redshift, $z = 1.0$, and shifted toward longer durations. The total number of bursts that satisfy the condition (21) is similar to that in Fig. 10 and about ~ 700 out of a 1000 bursts exhibit a large flux in gamma

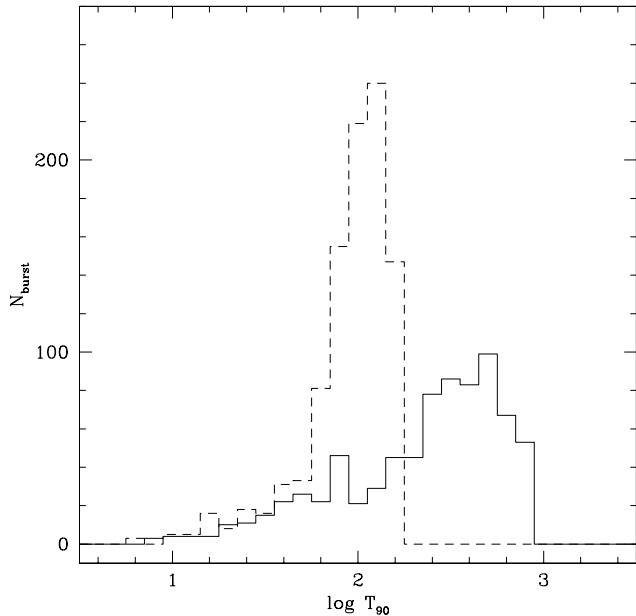


Figure 11. The same as in Fig. 10, but with a random redshift distribution included. The redshift for each burst was chosen between 0 and 4, with a probability distribution that traces the star formation rate, $R_{SF}(\Omega_M = 0.3, \Omega_\Lambda = 0.7)$.

rays. However, the durations of the bursts with the distribution of redshifts tend to be more equal, due to the linear dependence on $1 + z$. This makes the peak of the histogram flatter. The shift toward longer durations results from the fact the redshift distribution traces the star formation rate according to the function Rsf_2 in Porciani & Madau (2001) so the number of events with $z < 1.0$ is very small while saturates for large z . Therefore the long bursts can be longer, due to the contribution of bursts with $z > 1.0$, while the short bursts have similar durations to these in Fig. 10.

4 DISCUSSION AND CONCLUSIONS

The scenario in which the central engine of a GRB operates like a “shot-gun” emitting multiple narrow bullets was originally suggested by Heinz & Begelman (1999). Also, Fenimore et al. (1999) showed that the variability of GRB may be due to the breaking of the local spherical symmetry of the emitting shells. In this case the duration of the total event was determined by the time of activity of the central engine, and therefore connected with the progenitor type. The observational evidence for the association of the long GRBs with supernovae (Bloom et al. 2002; Stanek et al. 2003) support the collapsar model. The simulations of the jet propagating through the envelope of the collapsing star (e.g. Aloy et al. 2000; MacFadyen et al. 2001) show that the jet has an ultimate Lorentz factor of about 100-150 and an opening angle wider than $\sim 10^\circ$. The jet does not have a uniform structure in its density, velocity, pressure etc. These physical quantities have a certain distribution along with the angular distance from the jet axis, however, the gradients are not very sharp, and it is not certain if this scenario could result

in a separate “bullets” released from the center during the time of activity.

One of the possible scenarios is the quasi-universal structured jet model (e.g. Rossi et al. 2002; Zhang & Meszaros 2002; Lloyd-Ronning et al. 2004), in which the observed diversity of GRB properties is explained by a different viewing angle. The jet has a standard geometrical configuration, with a stable outflow channel but jet properties (e.g. Lorentz factor, energy flux) are distributed non-uniformly per solid angle within the cone.

This is in contrast with the simple jet models, in which the energy distribution within the cone was uniform (Rhoads, 1997; Panaitescu et al. 1998). These simple jets have been used to successfully explain the breaks in the GRB optical afterglow lightcurves (Moderski et al. 2000; Huang et al. 2000; Granot et al. 2002). Since the energy is collimated to different degrees in various bursts, the jet opening angle is the main parameter that drives the jet properties. Which mechanism drives the various collimation degree in various GRBs remains to be explained.

The model studied in the present work invokes a kind of a “shot-gun” model, with a fixed opening angle, and a Gaussian distribution of the subjet probability around the symmetry axis. In the case of assumed instantaneous emission the model is effectively quite close to a “shot-gun” scenario while in the case of extended emission (i.e. thick shell approximation) the emitting gas has definitively a jet-like appearance. However, the model is different from the single structured jet since the distribution of the directions of sub-jets contains the element of randomness. The underlying assumption is that the process of the jet formation is not stable, and an open jet channel may close up and be replaced with a new one. In this model the GRB properties depend significantly on the observer’s position.

We first analyzed the profiles of single pulses coming from separate sub-jets.

Observationally, such profiles were studied by Ryde & Svensson (2002) for $T_{90} > 2$ s bursts in BATSE sample. They found a good representation of single subpulse profiles with equation (20), and noticed a two-peak distribution of the index n : a higher peak around $n = 1$ and a lower peak around $n = 3$. We completed their analysis for $T_{90} < 2$ and found one peak below $n = 1$ but no significant traces of the second one. If we restricted ourselves to the data with the highest S/N ratio (above 30) perhaps we could see a slight relative enhancement at $n \sim 3$, but we have only 11 such events in the sample.

We compared these results with the theoretical profiles. Assuming instantaneous emission we obtained values of n between $n = 4$ and $n = 6$. However, the emission from thick shell with $R_{\min} = 10^{14}$ cm and $R_{\max} = 2 \times 10^{14}$ cm results in pulse profiles that are slightly wider in their rising part and have a different decay profiles. The corresponding distribution of the index n is much broader and peaks below $n = 1$. Therefore, the thick shell approximation seems to be a better representation of the observational data within the frame of the adopted model.

We next analyzed the question whether the adopted model can explain the apparent existence of the two classes of bursts: short and long.

We found that the multiple sub-jet model can reproduce the bimodal distribution of GRB durations only for

some specific conditions and parameters. In particular, this kind of distribution is reproduced if only the sub-jets that are seen on the line of sight can contribute to the GRB. When this assumption is released and all the sub-jets can contribute to the GRB (provided they give a sufficient flux in gamma-rays), the bimodal distribution is smeared. Furthermore, the bimodal distribution vanishes completely whenever we assume the emission from a thick shell from R_{\min} to R_{\max} instead of instantaneous emission at R_0 .

In the sub-jet model studied in this paper the duration time of the GRB depends on two parameters: (i) the radius of the emitting photosphere of a shell, r_0 (or, more specifically, its combination with the sub-jet opening angle, $\Delta\theta_{\text{sub}}$) and (ii) on the time of activity of the central engine, T_{dur} . The case (i) refers to the single sub-pulses detected by the observer, while the case (ii) is for the multiple sub pulses.

An important ingredient of the model is the multiplicity of the sub-jets. This is parameterized by the ratio of the solid angle covered by all the sub-jets to the solid angle covered by the whole jet: $\xi = (N_{\text{sub}} \times \Delta\theta_{\text{sub}}^2) / \Delta\theta_{\text{tot}}^2$. If this ratio is larger than unity, i.e. we have multiple sub-jets scattered with some, say, Gaussian, distribution around the jet axis, most of the bursts contain multiple pulses and the chance of detecting a single pulse is large only very close to the edge of the jet. For the standard parameters used throughout this article we had $\xi = 350 \times (0.02)^2 / (0.2)^2 = 3.5$. The duration of the GRB is governed then by the activity time T_{dur} , and the simulations show that the bimodal distribution is possible only for two distinct values of this activity time.

We have a different situation for $\xi \ll 1$. Most of the bursts will then contain only single pulses, and their duration is governed by the photospheric radius r_0 . We checked, that for extremely low multiplicity ($N_{\text{sub}} = 10$, which gives $\xi = 0.1$) the bimodal distribution duration can be recovered, both for instantaneous and extended shell emission (see Figure 12). However, a question arises, if in such a case we can really talk about the “multiple sub-jet model”. Also, the observed GRB pulse profiles would look totally different, as we would have mostly single or double spikes even for observers looking very close to the jet axis. The observations of long GRBs show something different: many of them exhibit a narrow substructure rather than couple of spikes.

To sum up, we suggest that an explanation of the bimodal duration distribution of the observed GRBs is possible rather on the basis of two independent kinds of sources responsible for short and long events. This is further justified by the fact that apart from many similarities, there are also systematic differences between long and short bursts, such as their spectral hardness or the systematically lower fluence in the case of short bursts.

ACKNOWLEDGMENTS

We thank Marek Sikora, Tomek Bulik and Michał Chodorowski for helpful discussions. This work was supported in part by grant No. PBZ 057/P03/2001 of the Polish Committee for Scientific Research.

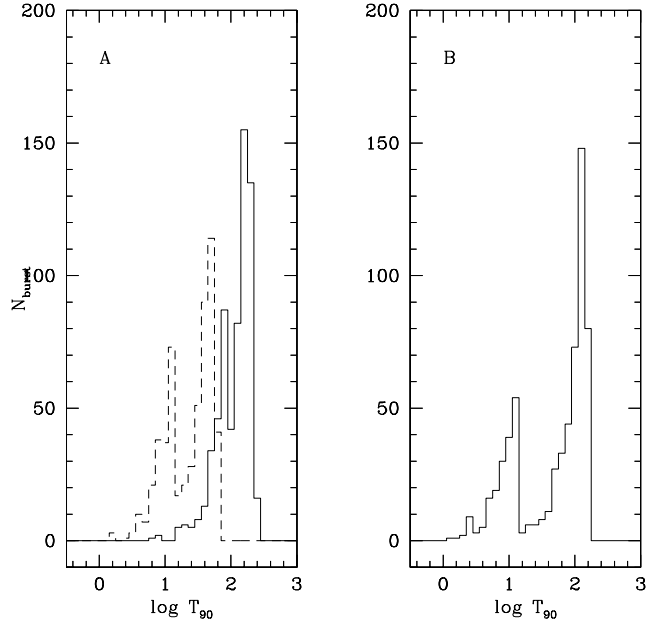


Figure 12. Histograms for models with very small sub-jet multiplicity: $N_{\text{sub}} = 10$, $\Delta\theta_{\text{sub}} = 0.02$, $\Delta\theta_{\text{tot}} = 0.2$. A: emission from $r_0 = 10^{14}$ cm (dashed line) and from $R_{\min} = 10^{14}$ cm to $R_{\max} = 2 \times 10^{14}$ cm (solid line); B: emission from $R_{\min} = 1.66 \times 10^{13}$ cm to $R_{\max} = 3.33 \times 10^{13}$ cm.

REFERENCES

- Aloy M.A., Muller E., Ibanez J.M., Marti J.M., MacFadyen A., 2000, ApJ, 531, L119
- Band D., et al., 1993, ApJ, 413, 281
- Berger E., et al., 2005, submitted to Nature (astro-ph/0508115)
- Bulik T., Belczyński K., Kalogera V., 2003, in Cruise M., Saulson P., eds, Proc. SPIE, Gravitational-Wave Detection. Int. Soc. Opt. Eng., Bellingham, WA, p. 146
- Bulik T., Gondek-Rosińska D., Belczyński K., 2004, MNRAS, 352, 1372
- Bloom J.S., Kulkarni S.R., Djorgovski, S.G., 2002, AJ, 123, 1111
- Burrows D.N. et al., 2005, GCN, 3494, 1
- Chodorowski M., 2005 (astro-ph/0407478)
- Eichler D., Livio M., Piran T., Schramm D.N., 1989, Nature, 340, 126
- Fenimore E.F., Madras C.D., Nayakshin S., 1996, ApJ, 473, 998
- Fenimore E.F., Cooper C., Ramirez-Ruiz E., Sumner M. C., Yoshida A., Namiki M., 1999, ApJ, 512, 683
- Fox D.B., et al., 2005, Nature, 437, 845
- Gehrels N., et al., 2005, Nature, 437, 851
- Ghirlanda G., Ghisellini G., Celotti A., 2004, A&A, 422, L55
- Granot J., Panaitescu A., Kumar P., Woosley S.E., 2002, ApJ, 570, L61
- Heinz S., Begelman M.C., 1999, ApJ, 527, L35
- Hjorth J., et al., 2005, Nature, 437, 859
- Horvath I., Meszaros A., Balazs L. G. Bagoly Z., 2004, BaltA, 13, 21
- Huang Y.F., Gou L.J., Dai Z.G., Lu T., 2000, ApJ, 543, 90

- Jakobsson P. et al, 2005, (astro-ph/0505542)
- Kosugi G., Furusawa H., Takada M., Kawai N., 2005, GCN, 3422, 1
- Kouvelietou C., et al., 1993, ApJ, 413, L101
- Lloyd-Ronning N., Dai X., Zhang B., 2004, ApJ, 601, 381
- MacFadyen A., Woosley S.E., Heger A., 2001, ApJ, 550, 410
- Moderski R., Sikora M., Bulik T., ApJ, 529, 151
- Narayan R., Paczyński B., Piran T., 1992, ApJ, 395, L83
- Paczynski B., 1998, ApJ, 494, L45
- Paczynski B., 1991, Acta Astron., 41, 257
- Panaitescu A., Meszaros P., Rees M.J., 1998, ApJ, 503, 314
- Pendleton G.N., et al., 1994, ApJ, 431, 416
- Piran T., 2004, Rev.Mod.Phys., 76, 1143
- Piro L., 2005, Nature, 437, 823
- Porciani C., Madau P., 2001, ApJ, 548, 522
- Preece R.D., et al., 1998, ApJ, 496, 849
- Preece R.D., et al., 2000, ApJS, 126, 19
- Prohaska J.X., Bloom J.S., Chen H.-W., Hurley K., 2005, GCN, 3399, 1
- Rees M.J., 1966, Nature, 211, 468
- Rhoads J.E., 1997, ApJ, 487, L1
- Rossi E., Lazzati D., Rees M.J., 2002, MNRAS, 332, 945
- Ryde & Svensson, 2002, ApJ, 566, 210
- Stanek K.Z., et al., 2003, ApJ, 591, L17
- Woosley S.E., 1993, ApJ, 405, 273
- Yamazaki R., Ioka K. Nakamura T., 2004, ApJ, 607, L103
- Toma K., Yamazaki R., Nakamura T., 2005, ApJ, 620, 835
- Villasenor J.S., et al., 2005, Nature, 437, 855
- Zhang B., Meszaros P., 2002, ApJ, 571, 876
- Zhang B., Meszaros P., 2004, Int.J.Mod.Phys., A19, 2385

